

Thin sea ice thickness as inferred from passive microwave and in situ observations

Kazuhiro Naoki,¹ Jinro Ukita,^{1,2} Fumihiko Nishio,¹ Masashige Nakayama,³ Josefino C. Comiso,⁴ and Al Gasiewski⁵

Received 7 April 2007; revised 10 October 2007; accepted 2 January 2008; published 19 February 2008.

[1] Microwave radiometric signals from sea ice strongly reflect physical conditions of a layer near the ice surface. This study examines the extent to which the relationships of thickness with brightness temperature and with emissivity hold for thin sea ice, approximately <0.2–0.3 m, and how those relationships may arise from changes in brine characteristics through modification of dielectric properties near the ice surface. In order to address these questions we made concurrent measurements of sea ice thickness in the Sea of Okhotsk from a ship and passive microwave radiometry from an over-flying aircraft. The results show that the brightness temperature and emissivity increase with thickness approximately within the thin ice for a frequency range of 10–37 GHz. The relationship is more pronounced at lower frequencies and at the horizontal polarization. We also established an empirical relationship between ice thickness and salinity in the layer near the ice surface from a field experiment, which qualitatively supports the idea that changes in the near-surface brine characteristics contribute to the observed thickness-brightness temperature/emissivity relationship. On the basis of our results, we conclude that for thin ice, passive microwave radiometric signals likely contain indirect information on ice thickness through the dependence of dielectric properties on brine, which provides a plausible and common explanation for previously proposed passive microwave thickness algorithms.

Citation: Naoki, K., J. Ukita, F. Nishio, M. Nakayama, J. C. Comiso, and A. Gasiewski (2008), Thin sea ice thickness as inferred from passive microwave and in situ observations, *J. Geophys. Res.*, 113, C02S16, doi:10.1029/2007JC004270.

1. Introduction

[2] The seasonal sea ice accounts for about 55% and 80% of the sea ice covers in the Northern and Southern Hemispheres, respectively [Gloersen *et al.*, 1992; Zwally *et al.*, 2002; Cavalieri *et al.*, 2003]. This implies that globally significant part of sea ice undergoes the stage of thin ice formation at one point within a seasonal cycle. It is estimated that the amount of heat flux through sea ice of thickness <0.5 m is 1 or 2 orders of magnitude higher than that through thicker ice types [Maykut, 1978]. In this context, it is highly significant that regions with critical climatic importance such as the subpolar North Atlantic and the Southern Ocean where dense water formation occurs are covered with seasonal sea ice. Model simulations also indicate that anomalous sea ice cover and thus heat fluxes could influence large-scale atmospheric circulation [Honda

et al., 1999; Alexander *et al.*, 2004]. From these considerations, accurate information on temporal and spatial distributions of thin ice is of significant importance to regional- and basin-scale heat budgets and atmosphere-ocean interaction. Despite the importance of thin ice it is difficult to obtain exact information on its thickness and spatial coverage. It remains a great challenge to derive thickness from satellite remote sensing. For altimeter measurements, necessary conversion from freeboard to total thickness makes it difficult to estimate thickness for thin ice [Kwok *et al.*, 2004]. Another approach is based on thermal infrared data from Advanced Very High Resolution Radiometer (AVHRR), in which ice thickness is estimated using the condition that the heat flux through the ice column equals to the atmospheric flux [e.g., Yu and Rothrock, 1996; Drucker *et al.*, 2003]. However, the method is limited by a large amount of uncertainty in the atmospheric heat flux over the seasonal sea ice zone. The approach based on SAR imagery focuses more on a growth history and requires careful interpretation in estimating ice thickness [Kwok *et al.*, 1999].

[3] It is also difficult to attain thickness information from passive microwave radiometry since the microwave emission from sea ice is mostly restricted to a layer of the top few centimeters, which depends on the wavelength of the radiation. Notwithstanding, previous work suggest that

¹Graduate School of Science and Technology and Center for Environmental Remote Sensing, Chiba University, Chiba, Japan.

²Now at Faculty of Science, Niigata University, Niigata, Japan.

³Kushiro Children's Museum, Hokkaido, Japan.

⁴NASA Goddard Space Flight Center, Greenbelt, Maryland, USA.

⁵Earth System Research Laboratory, Physical Science Division, NOAA, Boulder, Colorado, USA.

microwave radiometric signals carry information on ice thickness for thin ice, which is in this study referred to as ice with a thickness <0.3 m that includes nilas (thickness <0.1 m) and young ice (0.1–0.3 m of thickness) according to the WMO nomenclature [World Meteorological Organization, 2006]. Troy *et al.* [1981] report that the emissivity increases from nilas to young and to first-year ice (>0.3 m) [see Troy *et al.*, 1981, Figure 7]. Tucker *et al.* [1991] also present similar results [see Tucker *et al.*, 1991, Figure 8], while Eppler *et al.* [1992] summarize results from various field and laboratory experiments [see Eppler *et al.*, 1992, Table 4.1]. On the basis of the observation that a polarization ratio and a related brightness temperature ratio between vertical and horizontal polarization depend on thickness, algorithms are developed for classification of thin ice [e.g., Steffen, 1991; Cavaliere, 1994] and for estimation of thin ice thickness [e.g., Drucker *et al.*, 2003; Martin *et al.*, 2004, 2005]. While those studies consistently found the relationship between microwave radiometry and thickness, many of the field observations were not accompanied with exact information on thickness [Grenfell *et al.*, 1992]. Instead observations were often made with respect to sea ice types. Ambiguities remain owing to a low spatial resolution of space-borne measurements. Many of the previous observations suffer from ambiguities associated with the presence of open water areas and with a mixture of different ice types. What is needed is a focused field experiment on thin sea ice to measure passive microwave radiometry and thickness concurrently, which provides complementary information to laboratory experiments [e.g., Grenfell and Comiso, 1986].

[4] With this background the purpose of this study is to examine the relationship between the emissivity and thickness with a focus on the effects of changes in brine distribution. In particular, we examine the following questions: How robust is the relationship between passive microwave signature and thickness? Does the relationship hold for regions that have not been sampled previously? Is there any relationship between salinity in the layer near the ice surface and thickness in a field condition? If so, how much of the emissivity-thickness relationship is accounted for by emissivity dependence on brine characteristics? In order to address these questions, we analyzed data from concurrent airborne radiometric measurements with a field experiment which include thickness measurements from the ship in the Sea of Okhotsk in February 2003.

2. Experiment Description

2.1. Aircraft and Ship Observations

[5] Since 1995, sea ice and hydrographical observations have been made in the southernmost region of the Sea of Okhotsk using the icebreaker P/V *Soya* of the Japan Coast Guard [Toyota *et al.*, 1999; Ukita *et al.*, 2000]. During the 2003 cruise, from 6 to 15 February, a continuous survey on sea ice conditions was conducted from the ship (see Figure 1a for the location of the study area). In addition, passive microwave measurements were made from NASA's P3-B flying over the region on 7 February. Figure 1b shows the map of the observed brightness temperatures from the aircraft with ship's track indicated by the black line. As seen

in an Aqua/MODIS (Moderate Resolution Imaging Spectroradiometer) image (Figure 1c) taken at 1045 local time (LT) the sky was in clear condition, and the region was covered with sea ice with ice floes of various sizes.

[6] The P3-B flew from the Yokota Air Force Base in Japan and passed over the ship at 1102 LT at the altitude of 6000 m. Mounted on the aircraft is Polarimetric Scanning Radiometer (PSR). It is an airborne microwave imaging radiometer to obtain polarimetric microwave emission imagery of various surface components (see Piepmeier and Gasiewski [1996] and www.etl.noaa.gov/technology/psr for more detailed information). During our experiment, it measured brightness temperatures at the center frequencies of 10.7, 18.7, 21.5, 37.0, and 89.0 GHz and at both horizontal and vertical polarizations. The scanning swath was approximately 20 km. The size of the field of view (FOV) varies with frequency. Since the center position of each FOV is 150 m apart regardless of frequency, data were preprocessed and resampled for a meshed grid with the interval of 150 m. Figure 2 presents time series of the brightness temperatures at 18.7 and 37 GHz for both horizontal and vertical polarizations, which were constructed from the gridded data along ship's track using navigational information.

[7] At the ship, meteorological variables including wind direction and speed, air temperature, and humidity were recorded. Most importantly, sea ice conditions were continuously recorded using a video camera system, which consists of three cameras and a recorder (see Toyota *et al.* [1999] for the description of the system). Two cameras mounted at the bow and on the mast look into the forward direction, which provide visual information on sea ice conditions. In particular they inform us with the extent of homogeneity in sea ice conditions around the ship. The downward looking camera mounted at the side of the ship recorded images of the broken sea ice, from which sea ice thickness was estimated. Figure 3 presents thus obtained sea ice thickness distribution on 7 February (the day of the concurrent measurements).

2.2. Site Selection

[8] Thickness measurements from the ship were made throughout the day, while PSR measurements were made at around 1102 LT. This means that in the presence of ice motion a simple comparison between PSR pixels and ship's track based on their coregistered positions (e.g., latitude and longitude information) is misleading. In order to avoid sampling errors associated with this potential mismatch, we employed the following procedure.

[9] First, candidates for study sites were selected by visual inspection of the recorded video scene as well as a pair of MODIS and PSR images. In particular, we chose sites that meet the following criteria: (1) Sea ice concentration is nearly 100%; (2) the ice condition including thickness is close to constant; and (3) the above two conditions are satisfied over the distance of at least about 300 m along the track's direction and within the view from the ship. Second, we collocated those potential sites in the visible MODIS image (e.g., Figure 1b). This step was made possible by calm weather conditions. The potential sites were easily identified in the MODIS image based on ship's navigational data. In fact, the average wind speed during the

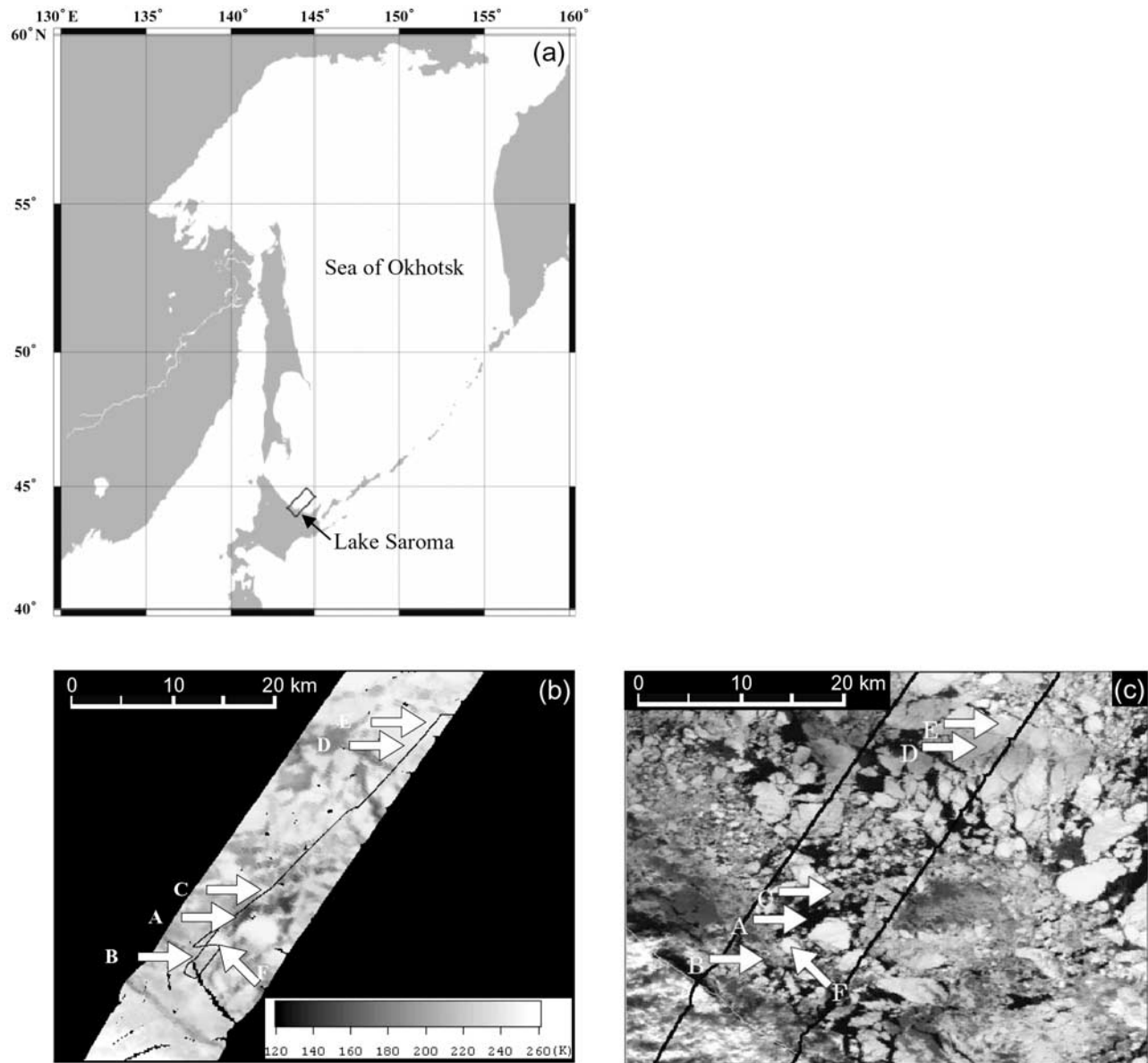


Figure 1. (a) Geographic location of the southern Sea of Okhotsk. The rectangular area indicates the PSR swath. (b) The 37-GHz H-polarization image from PSR in gray scale. The black line indicates ship's track. The locations of six sites are denoted as A to F. (c) Aqua/MODIS Channel 2 (841–876 nm) image. The locations of the study sites are denoted as in Figure 1b.

observation period was approximately 1.5 m/s. This translates to ice motion of 160 m per hour, assuming 3 percent as the ratio of ice to wind speeds. Since at this wind speed the nonlinear behavior of the steady state momentum balance would give a much smaller fraction this estimate is taken as a basis for maximum search distance in identifying targeted sites in the MODIS image (Figure 1c). The third step was to collocate those sites found in the MODIS image in the PSR brightness temperature image (e.g., Figure 1b) by a means of a visual inspection. This step was also made possible owing to a rather short interval between the times of the MODIS and PSR observations, for example, 17 min. The fourth step was to choose PSR grids for brightness temper-

ature measurements on the basis of the information gained through the above steps.

[10] By following the above procedure, we were able to measure thickness and brightness temperature from the same floe or a general area with highly homogeneous ice conditions. Our analysis indicates that this procedure, though not perfect, provides us with reasonably accurate matching between the locations of the PSR measurements and thickness measurements from the ship. In fact, on the basis of a four-way comparison between ship's video and navigational data, MODIS and PSR images, we confirmed that there was no substantial ice motion for Sites B and C. These sites represent the smallest in study area (short segments in ship's track) and were observed 3 and 4 hours

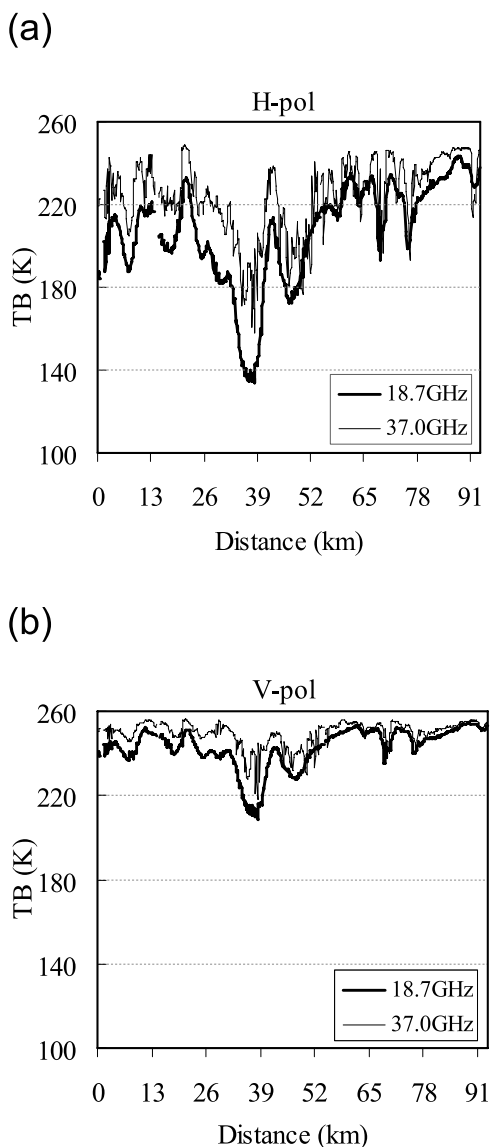


Figure 2. Time series of brightness temperatures along the flight path, (a) for the horizontal and (b) for vertical polarizations. The thick lines indicate the times series of 18.7 GHz, and the thin lines indicate 37.0 GHz. The values on the horizontal axes are approximate distances from the coast of Hokkaido.

prior to the time of the PSR observation. Hence the procedure appears to be reasonably valid.

[11] It turns out that six study sites are chosen. The mean sea ice thickness ranges from <0.05 m to about 0.3 m (Figures 1b and 1c indicate their locations in the brightness temperature map and the MODIS image, respectively). The mean ice thickness at Site B to F is 0.068 m, 0.111 m, 0.185 m, 0.272 m, 0.322 m, respectively (Table 1 gives the summary statistics). The thickness at Site A could not be determined from the video analysis, because it is only capable of estimating thickness >0.05 m. However, from the recorded video image it is confirmed that sea ice was present at Site A. Thus the nominal thickness of 0.025 m is

given for Site A. The sample size for thickness measurements varies from 12 to 99 depending on sites.

3. Results

3.1. Thickness Versus Brightness Temperature

[12] Figure 4 plots the mean brightness temperatures measured at the aircraft against the mean sea ice thickness measured for the six study sites for five frequencies, 10.7, 18.7, 21.5, 37.0, and 89.0 GHz, and for horizontal and vertical polarizations. A number of features are notable. (1) At all frequencies except 89 GHz, the brightness temperature increases with ice thickness for a thickness range up to 0.272 m. (2) At 89 GHz, the brightness temperature peaks at <0.2 m and decreases for the thickness >0.2 m. (3) The brightness temperature is lower for the horizontal polarization, and the difference between horizontal and vertical polarizations becomes smaller with increasing thickness (depolarization). (4) Except at 89 GHz, the brightness temperature is lower for lower frequency bands. (5) The positive relationship between the ice thickness and the brightness temperature is more pronounced with a steeper slope for the horizontal polarization and at lower frequencies (e.g., 10.7 GHz).

3.2. Thickness Versus Emissivity

[13] To account for the dependence of the brightness temperature on physical temperature of an emitting medium, it is desirable to discuss microwave signatures in terms of emissivity. To illustrate, Figures 5a and 5b (horizontal and vertical polarizations) plot emissivity against thickness for 6 sites and for 18.7 and 37 GHz. The plotted values are the brightness temperatures of Figure 4 divided by the physical temperature of 266.15 Kelvin (-7°C), which is the in situ ice surface temperature measured with a thermometer (Yokogawa, TX1003) at the time of the PSR overpass. A number of features are notable in Figures 5a and 5b. (1) The emissivity increases with ice thickness within the thin category. (2) Given an ice type and thickness, the emissivity is higher for the vertical polarization. (3) The variation in emissivity due to different polarizations diminishes with increasing thickness. (4) The variation in

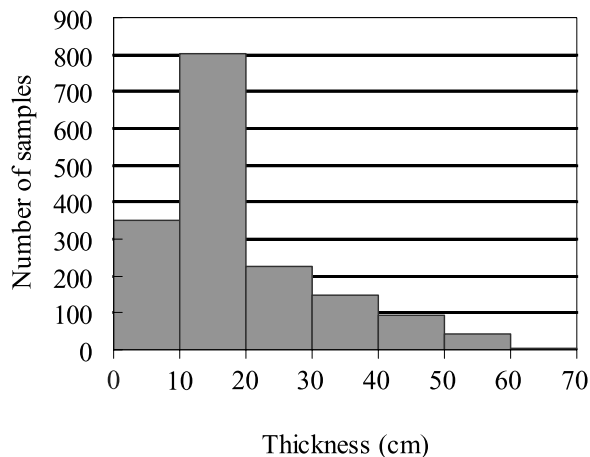


Figure 3. Sea ice thickness distribution from the ship's measurements on 7 February 2003. The mean thickness was 0.192 m from 1667 measurements.

Table 1. Summary of Thickness and Brightness Temperature Measurements^a

| | Site A | Site B | Site C | Site D | Site E | Site F |
|-------------------------------|-------------|-------------|-------------|-------------|-------------|-------------|
| Mean thickness, cm | 2.5 | 6.8(±1.1) | 11.1(±2.3) | 18.5(±3.8) | 27.2(±13.7) | 32.2(±7.4) |
| H-pol (K) | | | | | | |
| 10.7GHz | 119.1(±1.5) | 174.5(±1.3) | 190.3(±0.2) | 223.7(±1.7) | 231.7(±3.6) | 217.1(±9.3) |
| 18.7GHz | 137.7(±1.9) | 189.7(±0.9) | 211.1(±0.1) | 231.6(±1.8) | 240.4(±3.3) | 226.2(±7.0) |
| 21.5GHz | 154.0(±1.5) | 197.5(±1.3) | 222.5(±0.0) | 236.4(±1.5) | 244.3(±2.6) | 233.7(±6.7) |
| 37.0GHz | 175.1(±3.0) | 207.3(±0.3) | 235.2(±0.5) | 243.2(±1.7) | 246.3(±3.0) | 244.4(±7.6) |
| 89.0GHz | 196.2(±1.9) | 230.3(±0.3) | 233.7(±0.3) | 237.9(±1.3) | 227.6(±1.3) | 225.9(±2.8) |
| V-pol (K) | | | | | | |
| 10.7GHz | 196.1(±1.6) | 229.3(±0.7) | 236.2(±0.2) | 249.8(±3.2) | 249.5(±0.7) | 243.8(±5.1) |
| 18.7GHz | 212.6(±1.4) | 239.3(±0.9) | 242.0(±0.0) | 249.6(±1.3) | 253.6(±0.6) | 249.7(±1.5) |
| 21.5GHz | 217.6(±1.4) | 240.3(±0.5) | 244.2(±0.1) | 249.4(±1.1) | 253.5(±0.6) | 250.8(±1.4) |
| 37.0GHz | 230.2(±2.1) | 246.3(±0.5) | 248.9(±0.5) | 252.2(±0.6) | 254.9(±0.6) | 255.2(±1.1) |
| 89.0GHz | 243.5(±1.5) | 247.7(±1.0) | 246.9(±0.4) | 248.1(±1.5) | 238.3(±1.2) | 233.6(±3.6) |
| Number of samples (thickness) | N/A | 12 | 13 | 99 | 77 | 25 |
| Number of samples (PSR grids) | 7 | 3 | 3 | 25 | 23 | 7 |

^aAll values are averages for study sites A to F. The mean thickness for Site A was denoted as 2.5 cm, which was the half the measurement limit of 5 cm. The values inside the parentheses indicate corresponding standard deviations (1σ).

emissivity due to different polarizations is larger than that owing to different frequencies.

[14] There are uncertainties in the above estimates associated with the variations in ice thickness and brightness temperatures as seen in Table 1. Nevertheless, the thickness variation within each site is small enough such that there is no overlap between horizontal error bars among different sites/thickness except for the thickest point (Site F). The variation in the brightness temperature is also small. In converting from the brightness temperature to the emissivity, the values of the brightness temperatures are divided by the physical temperature. Ideally, the correct temperature to use is one that represents physical temperature of the emitting layer. This means that the temperature gradient within the ice column needs to be taken into account. In the absence of such information, we made a sensitivity analysis using the temperature range of -7°C to -1.8°C . As it turned out the maximum difference in emissivity when using -1.8°C instead of -7°C is about 0.02. The size of the

error bars is then estimated as the sum of 0.02 (due to temperature uncertainty) and the variation in brightness temperatures within each site (due to spatial homogeneity and represented by standard deviation in Table 1).

[15] In placing the above results in the context of the previous results, Figures 5c and 5d plot values of emissivity, which are compiled from other studies (the sources are found in the works of *Troy et al.* [1981], *Tucker et al.* [1991], and *Eppler et al.* [1992]). Many of those results are with respect to ice types such as nilas, new and young ice without thickness information. When exact thickness is not available, the representative (mean) thickness of each ice type is used. For example, 0.05 m and 0.2 m represent the thickness of nilas (<0.1 m) and young ice (0.1–0.3 m), respectively. Comparison of Figure 5a with Figure 5c and Figure 5b with Figure 5d shows a high degree of consistency, and common features are clearly identified. The most obvious feature is that the emissivity increases with ice thickness within the thin end, which is more pronounced for

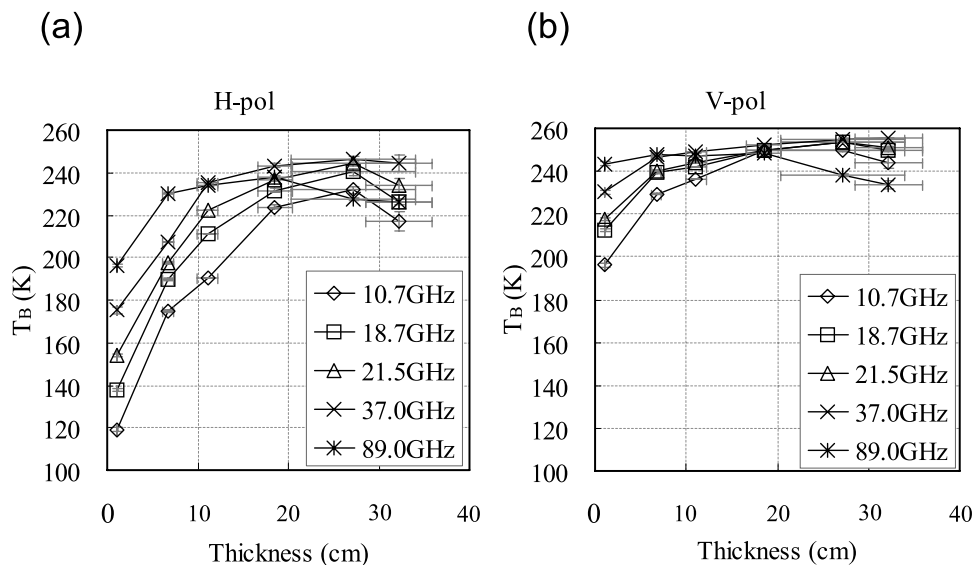


Figure 4. Thickness versus brightness temperatures for different frequencies and both (a) horizontal and (b) vertical polarizations. Horizontal and vertical bars indicate 1 standard deviation of ice thickness and brightness temperatures at each site.

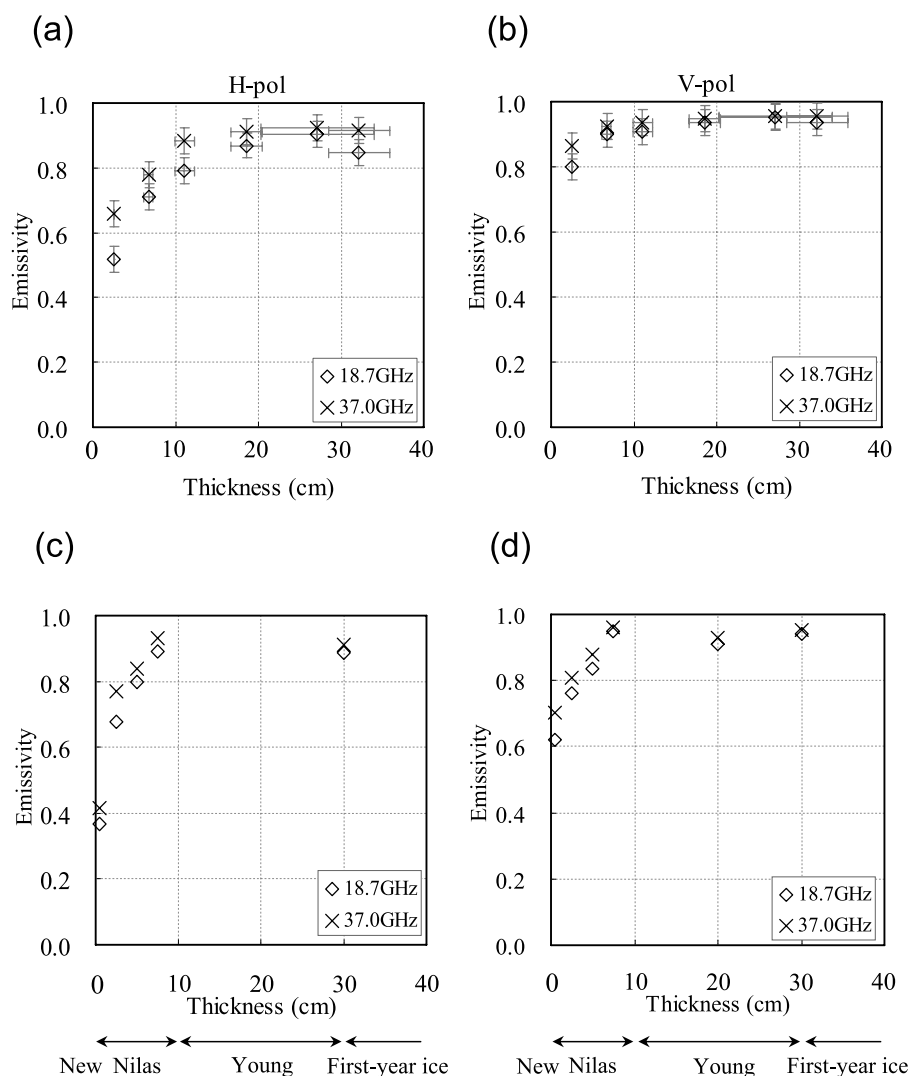


Figure 5. Comparison of thickness-emissivity relationships (a, b) from our observations and (c, d) from previous studies [Troy *et al.*, 1981; Tucker *et al.*, 1991; Eppler *et al.*, 1992]. For Figures 5c and 5d, mean values are used for different sea ice types according to the WMO nomenclature. See the text for the discussion on the error bars.

the horizontal polarization and for a lower frequency, for example, at 18.7 GHz. There are however some differences. For example, for the horizontal polarization our values are higher than the previously observed values for a thickness < 0.1 m.

4. Brine Hypothesis

4.1. Salinity-Thickness Relation

[16] For thin sea ice, evidence emerges that passive microwave radiometric signals contain indirect information on ice thickness. The brightness temperature increases with thickness when ice is approximately thinner than 0.2 m. This relationship has been observed consistently over different geographical locations including the central Arctic, the Bering Sea, the Greenland Sea, and the Sea of Okhotsk. This wide geographical distribution is taken as an indication that an underlying mechanism is fundamental in sea ice physics. Different factors such as influences from snow,

roughness, brine and temperature may contribute to this behavior in sea ice radiometry. However, given the consistency of the behavior across different observations, it may be argued that snow and temperature alone would not account for the observed relationship. This is because the amount of snow and temperature are highly variable in time and space owing to different weather and climatic conditions. Our analysis also suggests that the uncertainty in emissivity associated with the vertical temperature variation is small. It is unlikely that the low emissivity of the ocean beneath sea ice would account for the relationship, because the thickness range, for which the emissivity-thickness relation is observed, exceeds the penetration depth, for example, a wavelength. Having ruled out snow, temperature and the ocean as main attributes, we hypothesize that changes in brine with time and/or with thickness in freezing condition would be a main factor for the relationship (see the discussions in the works of Troy *et al.* [1981], Tucker *et al.* [1991] and Eppler *et al.* [1992]).

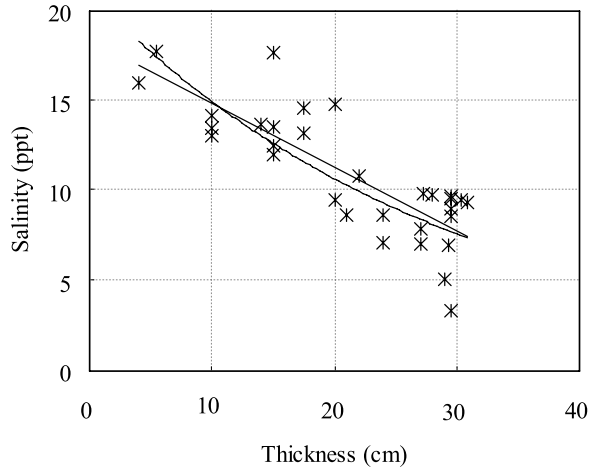


Figure 6. Relationship between sea ice thickness and surface (top 5 cm) salinity. All data were taken from various locations in Lake Saroma mostly from 1996 to 2004. The data for a thickness < 0.1 m were taken from a pool experiment in Lake Saroma in 2006. Two lines indicate regression lines according to linear and exponential forms.

[17] A physical basis for this brine hypothesis is observed dependence of salinity on ice thickness. It has long been known that there is a tendency that near-surface salinity decreases with the total thickness as a result of brine drainage [e.g., *Cox and Weeks, 1974; Ukita et al., 2000*]. In general, salinity near the ice surface tends to decrease in growing conditions and thus with time. We then explore the idea that the observed thickness-brightness temperature/emissivity relationship would reflect changes in dielectric properties associated with changes in brine characteristics. Ideally, testing this idea requires information on brine in the layer close to the surface concurrently with microwave radiometric and thickness measurements.

[18] As a step toward testing this idea, we conducted a field experiment at Lake Saroma. It is an ideal site to study sea ice in the southern Sea of Okhotsk, since the lake is connected to the Sea of Okhotsk with two open channels (Figure 1a) and shares sea ice and water properties including salinity with those outside. The experiments consisted with in situ measurements of salinity of the near-surface layer and ice thickness [see *Nakamura et al., 2006, Figure 7*].

[19] In Figure 6 the bulk salinity of the top 5 cm near the ice surface (when snow is present it is removed before taking an ice sample) is plotted against thickness. There appears a negative relationship between thickness and bulk salinity. In order to approximate functional dependence of near-surface salinity on thickness, least squares regression is applied to the data with two regression models. One is a linear model, which gives an estimated relationship as

$$S = 18.55 + 0.3678h, \quad (1a)$$

where S and h denote the bulk salinity of the top 0.05 m of the ice column and total thickness in centimeter. The other is an exponential model resulting in

$$S = 21.404e^{-0.0355h}. \quad (1b)$$

The above regression models explain 67% and 56% of the variance, respectively.

4.2. Modeling Temperature and Brine Effects

[20] In an attempt to quantify the extent to which changes in brine give rise to changes in emissivity through modification of dielectric properties, we examine a simplified two-phase mixture model of *Hoekstra and Cappillino [1971]*. Let e denotes the emissivity of sea ice, Γ the Fresnel reflection coefficient, θ the incidence angle from the nadir, and ε the dielectric constant.

$$e(\theta) = 1 - |\Gamma(\theta)|^2. \quad (2)$$

[21] The Fresnel reflection coefficient is expressed as

$$\Gamma(\theta) = \frac{\cos \theta - \sqrt{\varepsilon - \sin^2 \theta}}{\cos \theta + \sqrt{\varepsilon - \sin^2 \theta}} \quad (3a)$$

for the horizontal polarization and

$$\Gamma(\theta) = \frac{\varepsilon \cos \theta - \sqrt{\varepsilon - \sin^2 \theta}}{\varepsilon \cos \theta + \sqrt{\varepsilon - \sin^2 \theta}} \quad (3b)$$

for the vertical polarization. The complex dielectric constant for sea ice ε_{si} ,

$$\varepsilon_{si} = \varepsilon'_{si} + \varepsilon''_{si}, \quad (4)$$

can be modeled [*Hoekstra and Cappillino, 1971*] with

$$\varepsilon'_{si} = \frac{\varepsilon'_i}{1 - 3V_b} \quad (5a)$$

$$\varepsilon''_{si} = V_b \varepsilon''_b, \quad (5b)$$

where ε'_i (here assumed to be 3.15) is the real part of the dielectric constant for pure ice, ε''_b is the imaginary part of the dielectric constant for brine, and V_b is the brine volume. The ε''_b can be described as a function of frequency and physical parameters [e.g., *Stogryn, 1971; Ulaby et al., 1986*]. The brine volume can be related to salinity and temperature as

$$V_b = 10^{-3} S \left(\frac{-49.185}{T} + 0.532 \right), \quad (6)$$

where S and T and the bulk salinity in parts per thousand and temperature in the range of -0.5 to -22.9°C [*Frankenstein and Garner, 1967*]. Using (2) to (6) and the incidence angle of 55 degrees, the emissivity of sea ice can be modeled as a function of temperature and salinity. Now assuming the surface temperature of -7°C (in situ ice

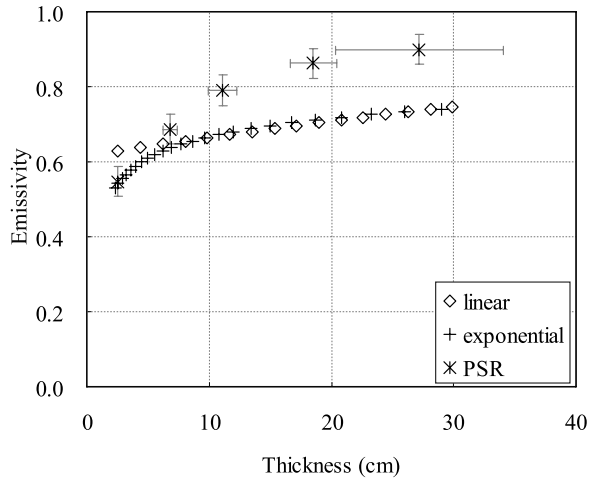


Figure 7. Comparison of thickness-emissivity relationships between our observations and model results. Diamond and plus symbols indicate the values based on the linear and exponential regression lines in Figure 6.

surface temperature as before) and linear and exponential thickness-salinity relationships (equations (1a) and (1b)), a thickness-emissivity relationship is modeled and compared with observed values (see Figure 7). The model results are qualitatively in agreement with the observations. In particular, both linear and exponential models explain a positive relationship between the brightness temperature and thickness. It is however noted that nonlinear behavior in PSR and other measurements for the thin end is only seen with an exponential model (equation (1b)). An important point derived from the above analysis is that the observed dependence of the brightness temperature and emissivity on thickness for thin ice can be at least partially explained by changes in brine distribution with age and thickness of ice, although contributions from other factors cannot be ruled out.

5. Discussions

[22] The above results support the notion that for thin ice the brightness temperature and emissivity of seasonal sea ice increase with ice thickness. Furthermore, the results from both field and modeling studies suggest that a plausible explanation for this relationship lies in changing brine distribution near the surface, which results in modification of dielectric properties and thereby leading to dependence of microwave radiometry on ice thickness.

[23] We now discuss the present results in conjunction with previous studies on a combined problem of classification of thin ice and estimation of its thickness. In particular we shall examine the approach that is based on passive microwave radiometry, in which microwave polarization information is utilized for classification of thin ice [Steffen, 1991; Cavalieri, 1994] and for thickness estimation [e.g., Drucker *et al.*, 2003; Martin *et al.*, 2004, 2005]. Let us define a polarization (PR) ratio and a spectral gradient (GR) ratio as

$$PR = \frac{T_b(19V) - T_b(19H)}{T_b(19V) + T_b(19H)} \quad (7a)$$

$$GR = \frac{T_b(37V) - T_b(19V)}{T_b(37V) + T_b(19V)} \quad (7b)$$

where T_b denotes the brightness temperature, and frequency and polarization are indicated inside the parentheses.

[24] On the basis of a series of tank and field experiments, Wensnahan *et al.* [1993] find that PR changes its value as ice grows. In particular they report a reversed sequence in PR values, i.e., an initial decrease followed by an increase in PR when ice grows to a thickness of about 0.06 m. Besides this, they find that the value of PR tends to be around 0.1 by the time ice grows to about 0.05 m. It is significant that this value is between the PR values of the open water and the first-year ice, which essentially serves as a basis for Cavalieri's thin ice algorithm [Cavalieri, 1994]. As he states, the question of this depolarization (decreasing PR toward zero) with ice thickness is not yet resolved. A particular difficulty arises from the fact that combined information of radiometry and thickness in the seasonal sea ice zone is scarce. Also, even if available, ambiguities remain as to possible biases from a mixture of different ice types and the open water.

[25] Keeping this background in mind, Figure 8 shows the values of PR and GR calculated on the basis of PSR measurements along with the thickness information. It is noted that PR values decrease with thickness except for the thickest case (0.32 m at Site F). In comparison, GR values are relatively unchanged and close to be zero. These results are highly consistent with the previous observations compiled in Table 1 of Cavalieri [1994]. More importantly, our results are from the observations with a less amount of ambiguities in terms of the mixing question.

[26] More recently, Martin *et al.* [2004] introduce an index called the Special Sensor Microwave/Imager (SSM/I) 37V/H ratio R_{37} defined as

$$R_{37} = \frac{T_b(37V)}{T_b(37H)}. \quad (8)$$

[27] They derived an empirical relationship of this ratio with ice thickness estimated from AVHRR data using the method described by Drucker *et al.* [2003]. The values of

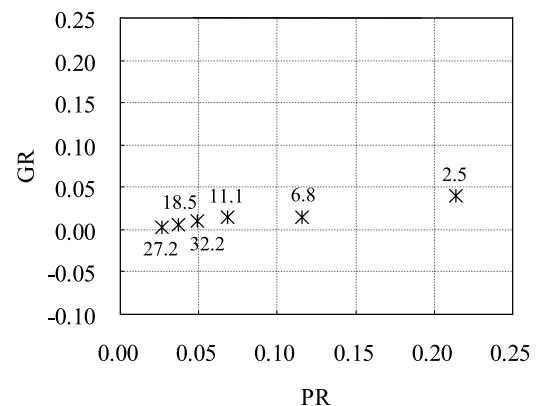


Figure 8. PR versus GR calculated from PSR measurements for six sites. The numerical values show the mean thickness at each site (e.g., Table 1).

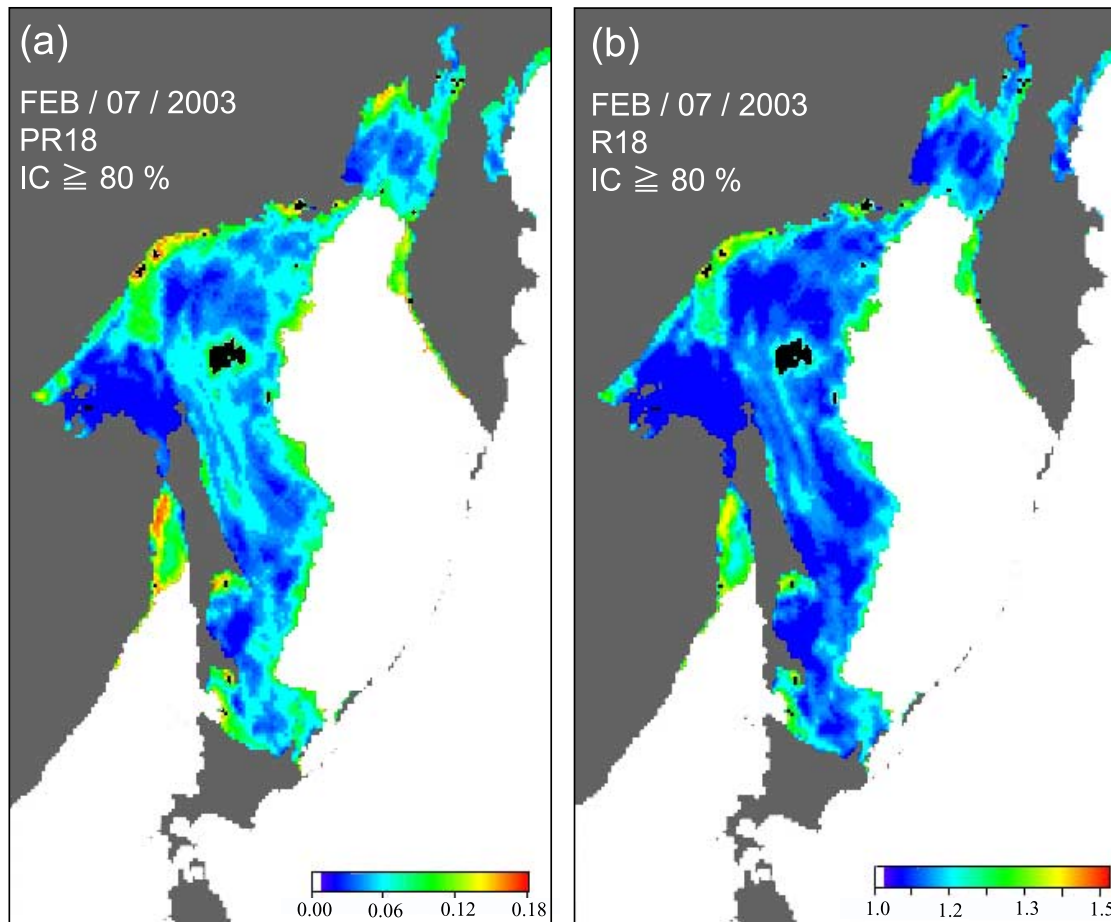


Figure 9. (a) Map of PR values based on AMSR-E observations on 7 February 2003 over the Sea of Okhotsk. (b) The same as Figure 9a but for the vertical to horizontal polarization ratio of brightness temperatures at 18 GHz (r_{18}). The areas with ice concentration $< 80\%$ within the sea ice boundary are masked out by black. The color scales indicate corresponding values.

R_{37} calculated from our PSR measurements range between 1.03 (Site D and E) to 1.31 (Site A). Qualitatively this range and its dependence on thickness (a negative relationship between thickness and R_{37}) are in agreement with those given by *Martin et al.* [2004]. It is also noted that R_{19} , which is the 19 GHz counterpart to R_{37} , has a wider range (1.05–1.54).

[28] To further compare our results with others, we map PR for 18 GHz and R_{18} using AMSR-E (The Advanced Microwave Scanning Radiometer–Earth Observing System) data for the entire Sea of Okhotsk on 7 February 2003 (Figure 9). Here in order to minimize influences from the open water, the only grids for which ice concentration are $> 80\%$ are considered [e.g., *Comiso et al.*, 2003]. Particular regions with high values, which are indicative of thin ice, are identified in both maps. One such an area is located along the northern coast, which is known to develop coastal polynyas [*Martin et al.*, 1998; *Shcherbina et al.*, 2004]. Other areas include two south-faced bays along the eastern coast of the Sakhalin Island, which are also known to be polynyas due to prevailing northerly winds and local topography. In all, those features are what we expect for a spatial pattern of the thin ice distribution over this region.

[29] Now focusing on our study region defined by the PSR swath (Figure 1), Table 2 presents statistics on PR and

R values for 18.7 GHz calculated from PSR measurements, which are geographically matching AMSR-E data for the same frequency. The minimum values of PR and R are similar between AMSR-E and PSR data (here the sample sizes are so different that standard statistical tests are not applied). The mean values are also close between the distributions derived from the two data sets. The maximum of PR values from PSR is notably larger (0.228) than that from AMSR-E. It is highly consistent with the value (0.275) found for the open water by *Cavalieri* [1994]. Similarly, the maximum of R values for PSR (1.593) is larger than that for AMSR-E. On the basis of the above comparisons, it appears that the present PSR measurements capture the same radiometric signature on thin ice thickness as the AMSR-E data do. Then our results are taken as evidence that a plausible physical explanation for previous passive microwave ice thickness algorithms lies in changing dielectric properties through changes in the near-surface brine characteristics.

6. Concluding Remarks

[30] The present results provide much needed ground truth for investigation of the relationship between passive microwave radiometry and ice thickness. In particular, they show the presence of the brightness temperature-thickness

Table 2. Comparison of PR and *R* Values Between AMSR-E and PSR Data

| | AMSR-E (n = 24) | PSR (n = 41777) |
|-------|-----------------|-----------------|
| PR18 | | |
| Range | 0.029–0.103 | 0.017–0.228 |
| Mean | 0.071 | 0.079 |
| R18 | | |
| Range | 1.060–1.230 | 1.034–1.593 |
| Mean | 1.154 | 1.177 |

relationship for thin ice accompanied by reasonably accurate information on thickness without ambiguity that might otherwise arise from a mixture of different ice types. Hence they provide a plausible physical basis for the algorithms of thin ice classification and estimation of thin ice thickness [Steffen, 1991; Cavalieri, 1994; Drucker et al., 2003; Martin et al., 2004, 2005].

[31] Our results point out the importance of near-surface brine distribution as a key factor for the dependence of microwave radiometry on thin ice thickness, which places a strong need for future in situ and concurrent measurements on radiometry, thickness, and brine characteristics. It is significant that the same physics is at work for both passive and active microwave sensors [Steffen and Heinrichs, 1994; Nakamura et al., 2006]. One way to extend our results is to consider other seasonal sea ice regions such as the Southern Ocean, for which efforts should be directed toward obtaining knowledge on brine distribution of sea ice under flooding and/or refreezing conditions. Last but not least importantly, more knowledge is needed on dielectric properties of sea ice in field conditions.

[32] **Acknowledgments.** We are grateful to the Japanese Coast Guard and *Soya's* crew for their assistance during the cruise. We also thank J. Inoue, K. Tateyama, T. Toyota, and S. Watanabe for their assistance and K. Nakamura and H. Wakabayashi for helpful discussions. Special thanks go to NASA and NOAA for providing observational opportunities.

References

- Alexander, M. A., U. S. Bhatt, J. E. Walsh, M. S. Timlin, J. S. Miller, and J. D. Scott (2004), The atmospheric response to realistic Arctic sea ice anomalies in an AGCM during winter, *J. Clim.*, *17*, 890–905.
- Cavalieri, D. J. (1994), Microwave technique for mapping thin sea ice, *J. Geophys. Res.*, *99*, 12,561–12,572.
- Cavalieri, D. J., C. L. Parkinson, and K. Y. Vinnikov (2003), 30-year satellite record reveals contrasting Arctic and Antarctic decadal sea ice variability, *Geophys. Res. Lett.*, *30*(18), 1970, doi:10.1029/2003GL018031.
- Comiso, J., D. Cavalieri, and T. Markus (2003), Sea ice concentration, ice temperature, and snow depth using AMSR-E data, *IEEE Trans. Geosci. Remote Sens.*, *41*(2), 243–252.
- Cox, G. F. N., and W. F. Weeks (1974), Salinity variations in sea ice, *J. Glaciol.*, *13*, 109–120.
- Drucker, R., S. Martin, and R. Moritz (2003), Observation of ice thickness and frazil ice in the St. Lawrence Island polynya from satellite imagery, upward looking sonar, and salinity/temperature moorings, *J. Geophys. Res.*, *108*(C5), 3149, doi:10.1029/2001JC001213.
- Eppler, D., et al. (1992), Passive microwave signature of sea ice, in *Microwave Remote Sensing of Sea Ice*, *Geophys. Monogr. Ser.*, vol. 68, edited by F. Carsey, chap. 4, pp. 47–71, AGU, Washington D. C.
- Frankenstein, G., and R. Garner (1967), Equations for determining the brine volume of sea ice from -0.5°C to -22.9°C , *J. Glaciol.*, *6*, 943–944.
- Gloersen, P., W. J. Campbell, D. J. Cavalieri, J. C. Comiso, C. L. Parkinson, and H. J. Zwally (1992), Arctic and Antarctic sea ice, 1978–1987: Satellite passive-microwave observations and analysis, *NASA Spec. Publ.*, *SP-511*, 290 pp.
- Grenfell, T. C., and J. C. Comiso (1986), Multifrequency passive microwave observations of first-year sea ice grown in a tank, *IEEE Trans. Geosci. Remote Sens.*, *GE-24*, 826–831.
- Grenfell, T. C., D. J. Cavalieri, J. C. Comiso, M. R. Drinkwater, R. G. Onstott, I. Rubinstein, K. Steffen, and D. P. Winebrenner (1992), Considerations for microwave remote sensing of thin sea ice, in *Microwave Remote Sensing of Sea Ice*, *Geophys. Monogr. Ser.*, vol. 68, edited by F. Carsey, pp. 291–301, AGU, Washington, D. C.
- Hoekstra, P., and P. Cappillino (1971), Dielectric properties of sea and sodium chloride ice at UHF and microwave frequencies, *J. Geophys. Res.*, *76*, 4922–4931.
- Honda, M., K. Yamazaki, H. Nakamura, and K. Takeuchi (1999), Dynamic and thermodynamic characteristics of atmospheric response to anomalous sea-ice extent in the Sea of Okhotsk, *J. Clim.*, *13*, 617–633.
- Kwok, R., G. F. Cunningham, N. LaBell-Hamer, B. Holt, and D. A. Rothrock (1999), Sea ice thickness from high-resolution SAR imagery, *Eos Trans. AGU*, *80*, 495–497.
- Kwok, R., H. J. Zwally, and D. Yi (2004), ICESat observations of Arctic sea ice: A first look, *Geophys. Res. Lett.*, *31*, L16401, doi:10.1029/2004GL020309.
- Martin, S., R. Drucker, and K. Yamashita (1998), The production of ice and dense shelf water in the Okhotsk Sea polynyas, *J. Geophys. Res.*, *103*, 27,771–27,782.
- Martin, S., R. Drucker, R. Kwok, and B. Holt (2004), Estimation of the thin ice thickness and heat flux for the Chukchi Sea Alaskan coast polynya from Special Sensor Microwave/Imager data, 1990–2001, *J. Geophys. Res.*, *109*, C10012, doi:10.1029/2004JC002428.
- Martin, S., R. Drucker, R. Kwok, and B. Holt (2005), Improvements in the estimates of ice thickness and production in the Chukchi Sea polynyas derived from AMSR-E, *Geophys. Res. Lett.*, *32*, L05505, doi:10.1029/2004GL022013.
- Maykut, G. (1978), Energy exchange over young sea ice in the central Arctic, *J. Geophys. Res.*, *83*, 3646–3658.
- Nakamura, K., H. Wakabayashi, S. Uto, K. Naoki, F. Nishio, and S. Uratsuka (2006), Sea-ice thickness retrieval in the Sea of Okhotsk using dual-polarization SAR data, *Ann. Glaciol.*, *44*, 261–268.
- Piepmeyer, J. R., and A. J. Gasiewski (1996), Polarimetric Scanning Radiometer for airborne microwave imaging studies, paper presented at 1996 International Geoscience and Remote Sensing Symposium, Inst. of Electr. and Electron. Eng., Lincoln, Neb.
- Shcherbina, A. Y., L. D. Talley, and D. L. Rudnick (2004), Dense water formation on the northwestern shelf of the Okhotsk Sea: 1. Direct observations of brine rejection, *J. Geophys. Res.*, *109*, C09S08, doi:10.1029/2003JC002196.
- Steffen, K. (1991), Energy flux density estimation over sea ice based on satellite passive microwave measurements, *Ann. Glaciol.*, *15*, 178–183.
- Steffen, K., and J. Heinrichs (1994), Feasibility of sea ice typing with Synthetic Aperture Radar: Merging of Landsat Thematic mapper and ERS-1 SAR satellite imagery, *J. Geophys. Res.*, *99*, 22,413–22,424.
- Stogryn, A. (1971), Equations for calculating the dielectric constant of saline water (Correspondence), *IEEE Trans. Microwave Theory Tech.*, *19*, 733–736.
- Toyota, T., J. Ukita, K. I. Ohshima, M. Wakatsuchi, and K. Muramoto (1999), A measurement of sea ice albedo over the southwestern Okhotsk Sea, *J. Meteorol. Soc. Jpn.*, *77*, 117–133.
- Troy, B. E., J. P. Hollinger, R. M. Lerner, and M. M. Wisler (1981), Measurement of the microwave properties of sea ice at 90GHz and lower frequencies, *J. Geophys. Res.*, *86*, 4283–4289.
- Tucker, W. B., III, T. C. Grenfell, R. G. Onstott, D. K. Perovich, A. J. Gow, R. A. Shuchman, and L. L. Sutherland (1991), Sea ice properties in the winter marginal ice zone, *J. Geophys. Res.*, *96*, 4573–4587.
- Ukita, J., T. Kawamura, N. Tanaka, T. Toyota, and M. Wakatsuchi (2000), Physical and stable isotopic properties and growth processes of sea ice collected in the southern Sea of Okhotsk, *J. Geophys. Res.*, *105*, 22,083–22,093.
- Ulaby, F. T., R. K. Moore, and A. K. Fung (1986), *Microwave Remote Sensing: Active and Passive*, vol. III, *From Theory to Applications*, pp. 1065–2137, Artech House, Norwood, Mass.
- Wensnahan, M., G. A. Maykut, T. C. Grenfell, and D. P. Winebrenner (1993), Passive microwave remote sensing of thin sea ice using principal component analysis, *J. Geophys. Res.*, *98*, 12,453–12,468.
- World Meteorological Organization (2006), WMO Sea Ice Nomenclature, *Rep. 259*, Geneva.
- Yu, Y., and D. A. Rothrock (1996), Thin ice thickness from satellite thermal imagery, *J. Geophys. Res.*, *101*, 25,753–25,766.
- Zwally, H. J., J. C. Comiso, C. L. Parkinson, D. J. Cavalieri, and P. Gloersen (2002), Variability of the Antarctic sea ice cover, *J. Geophys. Res.*, *107*(C5), 3041, doi:10.1029/2000JC000733.

J. C. Comiso, NASA Goddard Space Flight Center, Code 614.1, Greenbelt, MD 20771, USA. (josefino.c.comiso@nasa.gov)

A. Gasiewski, Earth System Research Laboratory, Physical Science Division, NOAA, 325 Broadway R/ETL, Boulder, CO 80305-3328, USA. (al.gasiewski@noaa.gov)

M. Nakayama, Kushiro Children's Museum, 10-2 Miyuki, Kushiro, Hokkaido 085-0017, Japan. (nakayama@kodomoyugakukan.jp)

K. Naoki and F. Nishio, Graduate School of Science and Technology and Center for Environmental Remote Sensing, Chiba University, 1-33 Yayoi, Chiba 950-2181, Japan. (naoki@restaff.chiba-u.jp; fnishio@faculty.chiba-u.jp)

J. Ukita, Faculty of Science, Niigata University, Ikarashi, Niigata 950-2181, Japan. (jukita@env.sc.niigata-u.ac.jp)